Editors' Suggestion

Microcavity Nonlinear Optics with an Organically Functionalized Surface

Jin-hui Chen,[1] Xiaoqin Shen,[2] Shui-Jing Tang,[1,3,4] Qi-Tao Cao,[1,3] Qihuang Gong,[1,3,4,5] and Yun-Feng Xiao[1,3,4,5,*]

[1]State Key Laboratory for Artificial Microstructures and Mesoscopic Physics, School of Physics, Peking University, Beijing 100871, China

[2]School of Physical Science and Technology, ShanghaiTech University, Shanghai 201210, China

[3]Frontiers Science Center for Nano-optoelectronics and Collaborative Innovation Center of Quantum Matter, Beijing 100871, China

[4]Collaborative Innovation Center of Extreme Optics, Shanxi University, Taiyuan 030006, China

[5]Beijing Academy of Quantum Information Sciences, Beijing 100193, China

(Received 22 April 2019; published 24 October 2019)

We report enhanced optical nonlinear effects at the surface of an ultrahigh-Q silica microcavity functionalized by a thin layer of organic molecules. The maximal conversion efficiency of third harmonic generation reaches $\sim 1680\%/\mathrm{W}^2$ and an absolute efficiency of 0.0144% at pump power of ~2.90 mW, which is approximately 4 orders of magnitude higher than that in a reported silica microcavity. Further analysis clarifies the elusive dependence of the third harmonic signal on the pump power in previous literature. Molecule-functionalized microcavities may find promising applications in high-efficiency broadband optical frequency conversion and offer potential in sensitive surface analysis.

DOI: 10.1103/PhysRevLett.123.173902

Ultrahigh-Q optical microcavities have become intriguing platforms for light-matter interactions owing to their strong confinement of a light field [1–3]. Recent years have witnessed broad applications of optical microcavities ranging from low-threshold microlasers to nonlinear optics to quantum optomechanics [4–7]. A notable feature of microcavities is the inherent leaking evanescent field at the surface, which not only enables efficient near-field waveguide coupling [8,9] but also promotes fundamental and practical applications [10–15]. Breakthroughs on exploring the surface effects of ultrahigh-Q microcavities have been realized, such as chiral quantum optics [16–18], single nanoparticle sensing [19–21], monolayer excitonic laser [22,23], and symmetry-breaking-induced nonlinear optics [24–26].

In particular, silica whispering-gallery microcavities are mainstay photonic devices for their intrinsically ultralow loss in the broadband spectra and the mature fabrication in modern technology [27–29], but unfortunately suffer from low second- and third-order optical nonlinearity. Alternatively, there is ever increasing interest in the surface functionalization strategy to bridge the microcavities with the vast library of nonlinear molecules, which aims to improve properties and expand applications of the bulk materials [30–34]. In this work, we report the enhanced third harmonic generation (THG) and third-order sum frequency generation (TSFG) at the surface of organically functionalized ultrahigh-Q silica microcavities. The highly challenging problem of optical mode dispersion is tackled with dynamic phase matching. Experimentally, a record conversion efficiency of $\sim 1680\%/\mathrm{W}^2$ is realized for the third harmonic (TH), which is comparable with that of state-of-the-art chip-integrated microring cavities [35]. Further analysis elucidates the distinct dependence of the output TH power on pump power in the literature [29,35–37].

Figure 1(a) shows that a silica microsphere with a diameter of ~62 μm is functionalized with a thin layer of 4-[4-diethylamino(styryl)] pyridinium (DSP) molecules [38] of high third-order nonlinear coefficient ($n_2 = 2.54 \times 10^{-17}$ m^2/W) [34]. The deposition of DSP molecules onto the microcavity surface is indicated by the photoluminescence spectrum in Fig. 1(b). The dual microfiber waveguides with diameters of about 1 and 0.6 μm are designed for the evanescent coupling of pump light (infrared) and harmonic signal (visible), respectively. Figure 1(c) plots infrared transmission spectra for nondegenerate transverse-electric (TE) and transverse-magnetic (TM) polarization modes, showing typical Q factors of about 1.9×10^7 and 2.9×10^7, respectively. In this study, the deposition of DSP molecules reduces the Q factor of microcavities by at most a factor of 3 [38].

When the functionalized microcavity is pumped at 1533.8 nm, the bright green TH signal is observed at 511.0 nm measured on an electron-multiplying CCD (Andor, newton$^{\mathrm{EM}}$) as shown in Fig. 1(d). The small deviation (~0.27 nm) of measured TH wavelength is within the resolution (~0.34 nm) of our spectrometer. Besides the TH signal, stimulated Raman scattering and parametric oscillation are also observed for a range of pump power [Figs. 1(d) and 3(c)]. The phase mismatch of waveguide-microcavity coupling may cause a significant reduction of the collection of TH signals [29,36,37].

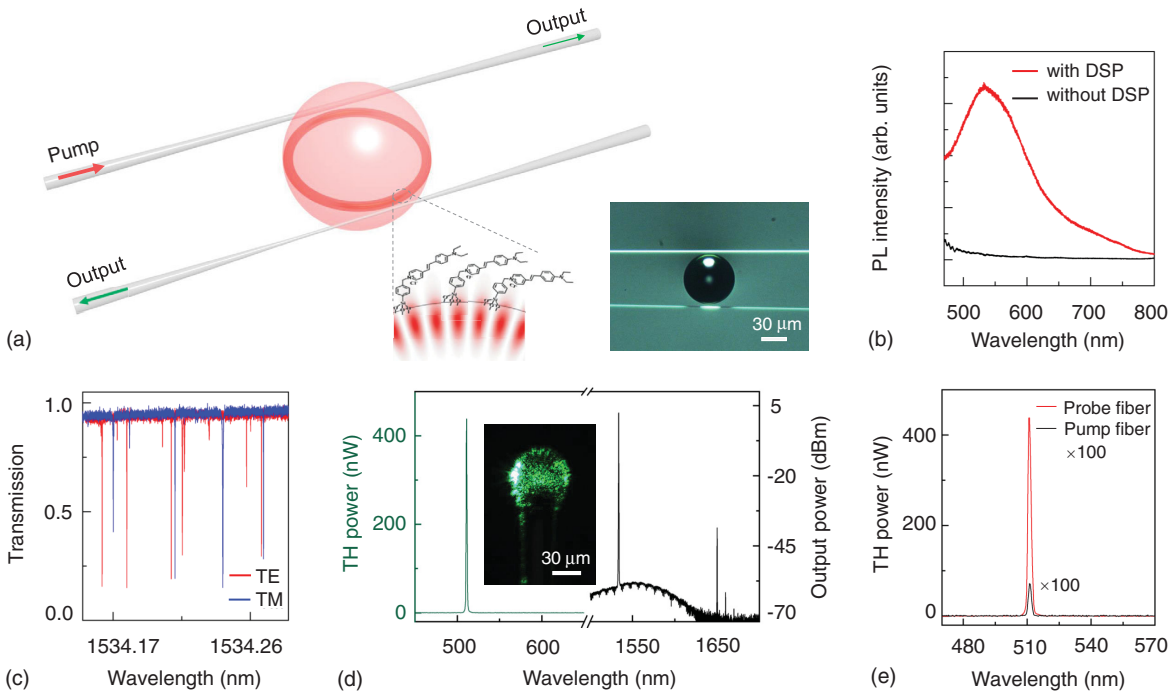

FIG. 1. (a) Schematic of the organically functionalized silica microsphere. Inset: Optical microscope image of microsphere coupled with dual microfibers. (b) Photoluminescence of silica substrate deposited with or without organic molecules. (c) Typical optical transmission spectra for TE and TM polarization modes in a functionalized microsphere. (d) Measured TH spectrum (green) and infrared pump spectrum (black). Inset: Scattering CCD image of the TH signal. (e) Comparison of the TH power collected by the probe fiber and pump fiber (100× magnified).

We thus optimize the fiber-microcavity coupling for both pump and probe fibers, and the collection efficiency by the probe fiber is found to be about 2 orders of magnitude larger than that by the pump fiber [Fig. 1(e)].

By solving nonlinear coupled-mode equations, the generated TH power (P_2) [38] is

$$P_2 = \frac{256|g|^2 Q_1^6 Q_2^2/(Q_{1e}^3 Q_{2e})}{\omega_1^3 \omega_2 [4Q_1^2(\frac{\omega_p}{\omega_1}-1)^2+1]^3 [4Q_2^2(\frac{3\omega_p}{\omega_2}-1)^2+1]} P_1^3, \quad (1)$$

where the subscripts $j = 1, 2$ indicate the pump and TH cavity modes with resonant angular frequencies ω_j, Q_j and Q_{je} are the loaded and external quality factors of a cavity mode, respectively, g is the third-order nonlinear coupling coefficient between the pump and TH cavity modes [38], which is composed of the nonlinearity from the bulk silica and surface molecules, and ω_p and P_1 are the angular frequency and input power of the pump light, respectively. Without regarding the explicit optical field distribution of pump and TH light, the nonzero g requires momentum conservation, i.e., $3m_1 = m_2$, where m_1 and m_2 are the angular mode number of the pump and TH field. From Eq. (1) it is found that, on the one hand, the ultrahigh Q boosts the TH conversion efficiency which scales $Q_1^3 Q_2$ in the double-resonance condition ($\omega_p = \omega_1 = \omega_2/3$); on the other hand, ultrahigh Q shrinks the optical window for phase matching. Note that the strategy in Ref. [41] compensates the phase mismatch in four-wave mixing by sophisticated optical mode engineering in a microring with a typical Q factor of 10^6. However, it is fundamentally challenging to transplant this technique to the ultrahigh-Q microcavities ($\sim 10^7$–10^8) for THG operated in a broad wavelength span.

Here, we show that the phase mismatch of the THG process can be compensated dynamically by thermal and optical Kerr effects [24,42]. To this end, we introduce the dimensionless parameter $\chi = (3\omega_1 - \omega_2)/\gamma_2$ to describe the dynamic phase mismatch for the THG process, where γ_2 is the linewidth of the TH cavity mode. In the cold cavity condition, the double resonance is usually unsatisfied due to the cavity geometry and material dispersions [29]. Thanks to the thermal and optical Kerr effects, the high intracavity pump power induces redshifts for both the pump and TH cavity modes. Generally, these effects introduce a larger resonance shift on the pump cavity mode than that of the TH mode, considering their spatial field distributions and overlap integrals [24].

Since the shift of the TH signal is linearly correlated to that of the pump mode in the case of resonance ($\omega_p = \omega_1$), the TH signal experiences a larger shift than its resonant mode, resulting in the reduction of χ with the increase of pump power, as shown in Fig. 2(a). Therefore, a critical pump power (P_c) appears at which both the pump light and

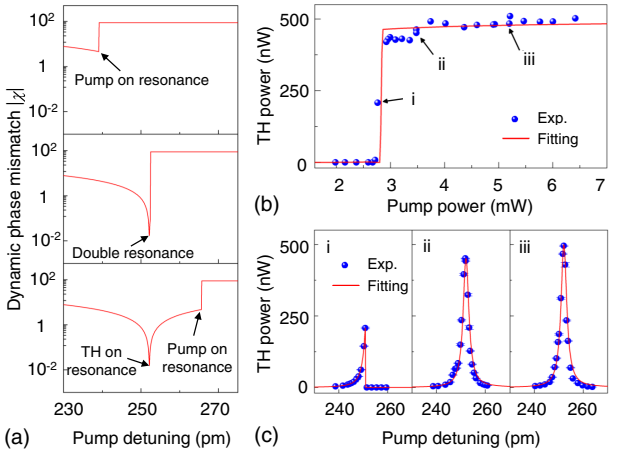

FIG. 2. (a) Dynamic phase mismatch parameter $|\chi|$ depending on the pump detuning with the cold cavity mode. From top to bottom, the pump power P_1 is set as 2.70, 2.85, and 3.00 mW. (b) Dependence of maximal output TH power on the input pump power. (c) Three typical spectra of TH power versus the pump detuning at different input power as indicated in (b). The theoretical fitting parameters in (b) and (c) are the same as that in (a), and can be found in Ref. [38].

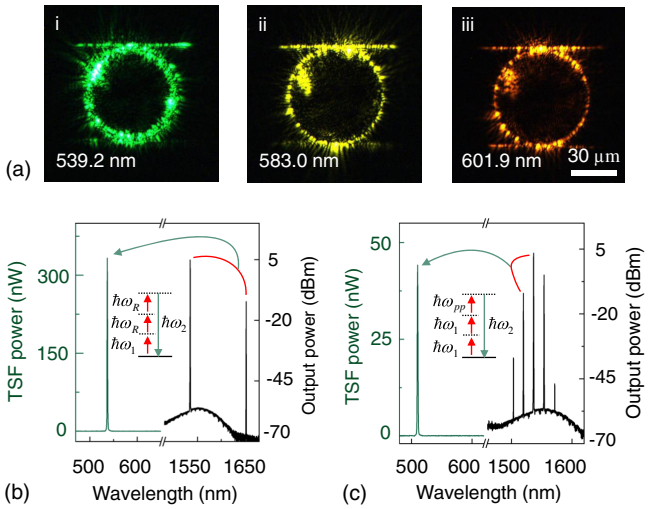

FIG. 3. (a) Observation of multicolor light emissions due to TSFG. (b) Measured spectra of Raman-scattering-assisted TSFG. One pump photon (ω_1) and two Raman Stokes photons (ω_R) are annihilated to create a visible photon (ω_2). (c) Measured spectra of parametric-oscillation-assisted TSFG. Two pump photons (ω_1) and one parametric photon (ω_{pp}) create a visible photon (ω_2).

TH signal can catch their hot resonant modes, and the double resonance is realized [middle panel, Fig. 2(a)]. Below the critical power, although the pump light can achieve resonance on its cavity mode, the TH signal remains in the blue-detuned state [upper panel, Fig. 2(a)]. The sharp increase of χ is due to the nonlinear bistability effect [42]. Above the critical power, the TH signal reaches the resonant state first, and so does the pump light with further pump detuning [bottom panel, Fig. 2(a)]. In this condition, the maximal output TH power is determined by the compromise of the pump light and the TH signal's phase match.

Experimentally, to characterize the power dependence of the TH output on the pump, we tune the pump wavelength and record the highest output TH power at each input power. When the pump power is below the critical value (~2.90 mW), the collected TH output power is weak [Fig. 2(b)] because the TH signal is far off resonance ($\chi \gg 1$) within the full tuning range of the pump light; when the pump power becomes higher than the critical value, a strong TH signal is observed since both the pump light and TH signal fall into the linewidths of their cavity modes. Notably, the maximal TH power is nearly stable beyond the critical pump power [see, e.g., states (ii) and (iii) in Figs. 2(b) and 2(c)]. This is because the maximal TH power occurs in the condition of the TH signal on resonance [$3\omega_p = \omega_2$, bottom panel in 2(a)] at which the intracavity pump power is nearly constant with the increasing input due to the thermal and Kerr effects [24,42]. Note that the distinct shape of the TH signal on pump detuning around the critical power is captured successfully, as shown in panel (i) of Fig. 2(c), which is predicted by the dynamic phase mismatched χ curve in the middle panel of Fig. 2(a).

From the experimental data in Fig. 2(b), the TH output exceeding 400 nW is obtained, and the maximal conversion efficiency (P_2/P_1^3) as high as 1680%/W^2 is observed around the critical pump power, approximately 4 orders of magnitude higher than that of the best-reported bare silica microsphere cavity [29]. The record high conversion efficiency is contributed by the strong nonlinearity of organic molecules and the ultrahigh-Q-resonant enhancement of both pump light and TH signal. Because of the small range of power for perfect phase matching, the maximal absolute efficiency (P_2/P_1) of THG reaches ~0.0144% at a pump power of ~2.90 mW. However, theoretically, by selecting an appropriate dispersion of microcavity to increase the critical pump power for phase matching, the absolute efficiency can be further improved.

The multiemissions from the functionalized microsphere cavity are also observed due to TSFG, as shown in Fig. 3(a). By tracking the output third-order sum frequency (TSF) spectra and pump spectra in the infrared, it is found that the origin of the TSF signals can be attributed to Raman-scattering-assisted and the parametric-oscillation-assisted processes. For example, Fig. 3(b) shows the spectrum of the TSF signal (536.76 nm), which is converted by the sum of the pump light (1534.68 nm) and first-order stimulated Raman scattering (1652.64 nm). Different Raman scattering based TSFGs are also observed [38]. In our experiment, the TSFG contributed by stimulated Raman scattering is commonly observed, owing to the broad Raman gain bandwidth of silica. By tuning the pump

wavelength and the microfiber coupling position, strong cascaded parametric oscillations also occur [Fig. 3(c)], where two pump photons (1536.546 nm) and one parametric photon (1519.68 nm) are converted into a visible photon (510.02 nm). The coherent interaction between parametric oscillation and TSFG can find applications in all-optical signal processing [43].

Furthermore, we find that the TH and TSF of the functionalized microsphere depends highly on the polarization of the pump light, which is, in principle, absent in bare isotropic silica microsphere cavities. Experimentally, by pumping different modes with preidentified polarizations (TE and TM) and the fixed pump power, we record the output power of THG or TSFG under optimal fiber coupling. Figures 4(a) and 4(b) compare the pump polarization dependence of nonlinear frequency conversion for the surface functionalized and bare silica microsphere cavities, respectively. It is found that the output TH or TSF power with TE-polarized pump is on average about 2 orders of magnitude higher than that with TM-polarized pump in the surface functionalized microcavity [Fig. 4(a)]. In contrast, no significant polarization extinction is found for the third-order nonlinear frequency conversion in a bare silica microsphere of comparable size [Fig. 4(b)]. Since the dipole moments of DSP molecules tend to be aligned along the tangential plane of the microsphere surface by our fabrication processes [38], the molecule nonlinear polarization enhancement for TE pump modes in a functionalized microcavity is much higher than that for TM pump modes, qualitatively. Besides the polarization effects, Fig. 4 also indicates that the THG and TSFG of a surface functionalized microcavity are on average over 100 times larger than that of a bare microcavity under the same conditions, which reasonably agrees with the theoretical calculations [38].

Finally, we note that besides our results, different power dependences of THG have been reported in whispering-gallery microcavities [29,35–37]. To this end, we would elucidate more generally the dependence of output TH power (P_2) on the input power (P_1). As aforementioned, before the reach of critical power (P_c) for the double resonance, the maximal output power P_2 is obtained in the case of pump on resonance ($\omega_p = \omega_1$); thus, Eq. (1) can be rewritten as

$$P_2 \propto P_1^3/[4(\chi_0 - \Delta\chi)^2 + 1] = P_1^3/[4(\chi_0 - \eta P_1)^2 + 1], \quad (2)$$

where $\chi_0 = (3\omega_{10} - \omega_{20})/\gamma_2$ is the normalized initial phase mismatch, ω_{10} (ω_{20}) the resonant angular frequency of a cold cavity mode for the pump light (TH signal), $\Delta\chi = \eta P_1$ represents the compensation of phase mismatch due to the thermal and optical Kerr effects, and η is a power independent coefficient [38]. In particular, it can be found that when $\Delta\chi \equiv 0$, indicating the synchronous redshift of pump and TH cavity modes with the increasing pump power, the TH power manifests an exact cubic dependence on the pump power, i.e., $P_2 \propto P_1^3/(4\chi_0^2 + 1)$.

Generally, with a nonvanishing $\Delta\chi$, the dependence of TH power P_2 on pump power P_1 is illustrated in Fig. 5(a). When the TH signal is far off resonance ($\chi_0 > 1$) and the pump power is weak ($\Delta\chi \ll \chi_0$), a quasicubic dependence can be obtained as demonstrated by a uniform interval of P_2 contour curves with a fixed χ_0. When the pump power is approaching critical value P_c ($\chi_0 \sim \Delta\chi > 1$), the power dependence deviates from the cubic shape seriously with a shrinking interval of contour curves, and the specific P_2-P_1 power curves around P_c are shown by Fig. 5(b). As for the case of a nearly resonant TH signal with its cavity mode ($\chi_0 \ll 1$), a quasicubic dependence can be reached [black curve in Fig. 5(b)]. So far, the power dependence of TH on pump has been elucidated before the critical power. When the pump power is beyond P_c [gray region in Fig. 5(a)], Eq. (2) will break down, and the P_2-P_1 relation is fundamentally determined by the compromise of phase matching of both pump light and TH signal [bottom panel,

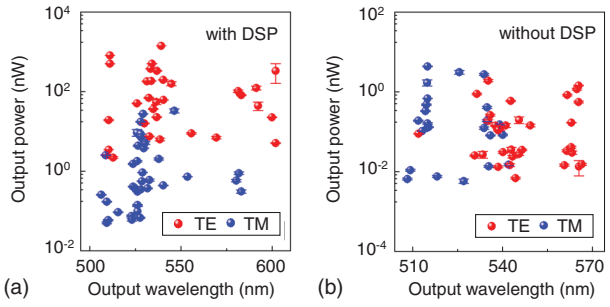

FIG. 4. Map of third-order nonlinear frequency conversion (TH and TSF) in (a) a surface functionalized silica microcavity and (b) a bare silica microcavity. The loaded Q factor of pump cavity mode is about 2.0×10^7 in (a) and 2.4×10^7 in (b). The pump power is kept the same (~7.5 mW), and the coupling conditions are optimized for TE and TM polarizations.

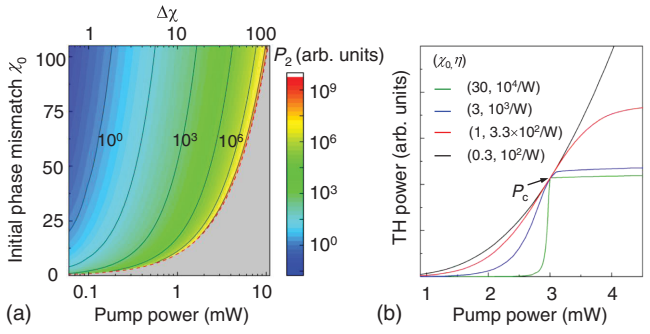

FIG. 5. (a) Contour diagram of TH output power P_2 dependence on the initial phase mismatch χ_0 and pump power P_1 with η of 10^4/W. The red dashed curve is the critical pump power (P_c) for double resonance, while the gray region beyond P_c can not be described by Eq. (2). (b) Maximal TH power dependence on pump power at different parameters of (χ_0, η).

Fig. 2(a)]. Thus, various curve shapes occur such as cubic, constant, linear dependence, etc. [Fig. 5(b) and Ref. [38]] by different parameters.

In summary, we have reported the highly efficient THG in a surface functionalized silica microcavity. The challenging phase matching is realized by leveraging the cavity-enhanced thermal and Kerr effects. The synergetic effect of surface modification and phase matching boost a record conversion efficiency of TH as high as $1,680\%/\mathrm{W}^2$. Moreover, we clarify the distinct dependence of TH power on the pump power reported in previous literature. This work unambiguously demonstrates the great potential of a surface functionalization strategy to manipulate and enhance the optical nonlinearity in microcavities, which is promising for tunable photonic devices and sensitive surface molecule sensing.

We thank Hao-Jing Chen, Xiao-Chong Yu, Yan-Jun Qian, and Liyun Zhao for helpful discussions and experimental assistance. This project was supported by the National Key R&D Program of China (Grants No. 2016YFA0301302 and No. 018YFB2200401) and NSFC (Grants No. 11825402, No. 11654003, No. 61435001, and No. 11527901), and High-performance Computing Platform of Peking University. X. S. was supported by the ShanghaiTech University startup funding (2019F0201-000-03). J.-h. C. was supported by the China Postdoctoral Science Foundation (Grant No. 2018M640015).

J.-h. C. and X. S. contributed equally to this work. X. S. fabricated the molecule-functionalized microsphere. J.-h. C. performed the experiment. S.-J. T. and J.-h. C. set up the measurement system. J.-h. C. and Q.-T. C. built the theoretical model. Y.-F. X. designed the experiment and supervised the project. All authors contributed to the discussion, analyzed the data, and wrote the manuscript.

*yfxiao@pku.edu.cn
www.phy.pku.edu.cn/~yfxiao/

[1] K. J. Vahala, Nature (London) **424**, 839 (2003).
[2] A. B. Matsko and V. S. Ilchenko, IEEE J. Sel. Top. Quantum Electron. **12**, 3 (2006).
[3] H. Cao and J. Wiersig, Rev. Mod. Phys. **87**, 61 (2015).
[4] L. He, Ş. K. Özdemir, and L. Yang, Laser Photonics Rev. **7**, 60 (2013).
[5] D. V. Strekalov, C. Marquardt, A. B. Matsko, H. G. Schwefel, and G. Leuchs, J. Opt. **18**, 123002 (2016).
[6] G. Lin, A. Coillet, and Y. K. Chembo, Adv. Opt. Photonics **9**, 828 (2017).
[7] M. Aspelmeyer, T. J. Kippenberg, and F. Marquardt, Rev. Mod. Phys. **86**, 1391 (2014).
[8] J. C. Knight, G. Cheung, F. Jacques, and T. Birks, Opt. Lett. **22**, 1129 (1997).
[9] S. M. Spillane, T. J. Kippenberg, O. J. Painter, and K. J. Vahala, Phys. Rev. Lett. **91**, 043902 (2003).
[10] H.-J. Moon, Y.-T. Chough, and K. An, Phys. Rev. Lett. **85**, 3161 (2000).
[11] B. Peng, Ş. K. Özdemir, F. Lei, F. Monifi, M. Gianfreda, G. L. Long, S. Fan, F. Nori, C. M. Bender, and L. Yang, Nat. Phys. **10**, 394 (2014).
[12] L. Chang, X. Jiang, S. Hua, C. Yang, J. Wen, L. Jiang, G. Li, G. Wang, and M. Xiao, Nat. Photonics **8**, 524 (2014).
[13] J. K. Poon, J. Scheuer, Y. Xu, and A. Yariv, J. Opt. Soc. Am. B **21**, 1665 (2004).
[14] Q. Song, Sci. China Phys. Mech. Astron. **62**, 074231 (2019).
[15] F. Xie, N. Yao, W. Fang, H. Wang, F. Gu, and S. Zhuang, Photonics Res. **5**, B29 (2017).
[16] C. Junge, D. O'Shea, J. Volz, and A. Rauschenbeutel, Phys. Rev. Lett. **110**, 213604 (2013).
[17] I. Shomroni, S. Rosenblum, Y. Lovsky, O. Bechler, G. Guendelman, and B. Dayan, Science **345**, 903 (2014).
[18] P. Lodahl, S. Mahmoodian, S. Stobbe, A. Rauschenbeutel, P. Schneeweiss, J. Volz, H. Pichler, and P. Zoller, Nature (London) **541**, 473 (2017).
[19] F. Vollmer and S. Arnold, Nat. Methods **5**, 591 (2008).
[20] M. R. Foreman, J. D. Swaim, and F. Vollmer, Adv. Opt. Photonics **7**, 168 (2015).
[21] Y. Zhi, X.-C. Yu, Q. Gong, L. Yang, and Y.-F. Xiao, Adv. Mater. **29**, 1604920 (2017).
[22] O. Salehzadeh, M. Djavid, N. H. Tran, I. Shih, and Z. Mi, Nano Lett. **15**, 5302 (2015).
[23] Y. Ye, Z. J. Wong, X. Lu, X. Ni, H. Zhu, X. Chen, Y. Wang, and X. Zhang, Nat. Photonics **9**, 733 (2015).
[24] X. Zhang, Q.-T. Cao, Z. Wang, Y.-x. Liu, C.-W. Qiu, L. Yang, Q. Gong, and Y.-F. Xiao, Nat. Photonics **13**, 21 (2019).
[25] J. S. Levy, M. A. Foster, A. L. Gaeta, and M. Lipson, Opt. Express **19**, 11415 (2011).
[26] M. Asano, S. Komori, R. Ikuta, N. Imoto, Ş. Özdemir, and T. Yamamoto, Opt. Lett. **41**, 5793 (2016).
[27] D. Armani, T. Kippenberg, S. Spillane, and K. Vahala, Nature (London) **421**, 925 (2003).
[28] Y.-S. Park, A. K. Cook, and H. Wang, Nano Lett. **6**, 2075 (2006).
[29] D. Farnesi, A. Barucci, G. C. Righini, S. Berneschi, S. Soria, and G. Nunzi Conti, Phys. Rev. Lett. **112**, 093901 (2014).
[30] G. Kozyreff, J. L. Dominguez-Juarez, and J. Martorell, Laser Photonics Rev. **5**, 737 (2011).
[31] J. L. Dominguez-Juarez, G. Kozyreff, and J. Martorell, Nat. Commun. **2**, 254 (2011).
[32] I. Kandas, B. Zhang, C. Daengngam, I. Ashry, C.-Y. Jao, B. Peng, S. K. Ozdemir, H. D. Robinson, J. R. Heflin, L. Yang, and Y. Xu, Opt. Express **21**, 20601 (2013).
[33] Y. Xu, M. Han, A. Wang, Z. Liu, and J. R. Heflin, Phys. Rev. Lett. **100**, 163905 (2008).
[34] X. Shen, R. C. Beltran, V. M. Diep, S. Soltani, and A. M. Armani, Sci. Adv. **4**, eaao4507 (2018).
[35] J. B. Surya, X. Guo, C.-L. Zou, and H. X. Tang, Optica **5**, 103 (2018).
[36] T. Carmon and K. J. Vahala, Nat. Phys. **3**, 430 (2007).
[37] X. Jiang, L. Shao, S.-X. Zhang, X. Yi, J. Wiersig, L. Wang, Q. Gong, M. Lončar, L. Yang, and Y.-F. Xiao, Science **358**, 344 (2017).

[38] See Supplemental Material at http://link.aps.org/supplemental/10.1103/PhysRevLett.123.173902 for details, which includes Refs. [39,40].

[39] F. Pan, M. S. Wong, C. Bosshard, and P. Günter, Adv. Mater. **8**, 592 (1996).

[40] P. Günter, Nonlinear Optical Effects and Materials (Springer-Verlag, Berlin, Heidelberg, 2000), Vol. **72**, p. 74.

[41] X. Lu, G. Moille, Q. Li, D. A. Westly, A. Singh, A. Rao, S.-P. Yu, T. C. Briles, S. B. Papp, and K. Srinivasan, Nat. Photonics **13**, 593 (2019).

[42] T. Carmon, L. Yang, and K. J. Vahala, Opt. Express **12**, 4742 (2004).

[43] X. Guo, C.-L. Zou, L. Jiang, and H. X. Tang, Phys. Rev. Lett. **120**, 203902 (2018).